Magnon crystallization in the kagomé lattice antiferromagnet

Jürgen Schnack,[1, *] Jörg Schulenburg,[2] Andreas Honecker,[3, †] and Johannes Richter[4, 5, ‡]

[1]*Fakultät für Physik, Universität Bielefeld, Postfach 100131, D-33501 Bielefeld, Germany*
[2]*Universitätsrechenzentrum, Universität Magdeburg, D-39016 Magdeburg, Germany*
[3]*Laboratoire de Physique Théorique et Modélisation, CNRS UMR 8089,*
CY Cergy Paris Université, F-95302 Cergy-Pontoise Cedex, France
[4]*Institut für Physik, Universität Magdeburg, P.O. Box 4120, D-39016 Magdeburg, Germany*
[5]*Max-Planck-Institut für Physik Komplexer Systeme,*
Nöthnitzer Straße 38, D-01187 Dresden, Germany
(Dated: June 11, 2020)

We present numerical evidence for the crystallization of magnons below the saturation field at non-zero temperatures for the highly frustrated spin-half kagomé Heisenberg antiferromagnet. This phenomenon can be traced back to the existence of independent localized magnons or equivalently flat-band multi-magnon states. We present a loop-gas description of these localized magnons and a phase diagram of this transition, thus providing information for which magnetic fields and temperatures magnon crystallization can be observed experimentally. The emergence of a finite-temperature continuous transition to a magnon-crystal is expected to be generic for spin models in dimension $D > 1$ where flat-band multi-magnon ground states break translational symmetry.

Introduction.—Strongly correlated electronic spin systems may possess unusual and thus attractive properties such as magnetization curves characterized by sequences of magnetization plateaus with possible crystallization of magnons as reported for Cd-kapellasite recently [1]. This is of course a consequence of the intricate nature of their many-body eigenstates [2–5], which, however, for, e.g., Hubbard as well as Heisenberg models under special circumstances can express itself as destructive interference that "can lead to a disorder-free localization of particles" [6]. For translationally invariant systems this automatically yields flat bands in the single-particle energy spectrum, i.e., in one-magnon space in the case of spin Hamiltonians [7–14]. Today, flat-band physics is investigated in several areas of physics, and many interesting phenomena that are related to flat bands have been found, see, e.g., Refs. [15–20]. Flat-band systems can also be created using, e.g., cold atoms in optical lattices [21, 22] or by employing photonic lattices [23–25].

Among the flat-band systems, the highly frustrated quantum antiferromagnets (AFMs) play a particular role as possible solid-state realizations. There is a large variety of one-, two-, and three-dimensional lattices, where at high magnetic fields the lowest band of one-magnon excitations above the ferromagnetic vacuum is completely flat [26, 27]. These flat-band antiferromagnets exhibit several exotic features near saturation, such as a macroscopic magnetization jump at the saturation field [10], a magnetic-field driven spin-Peierls instability [28], a finite residual entropy at the saturation field [13, 14, 29], a very strong magnetocaloric effect [14, 26, 30], and an additional low-temperature maximum of the specific heat signaling the appearance of an additional low-energy scale [26].

The focus of the present Letter is on a prominent example of a flat-band spin system, the spin-half kagomé
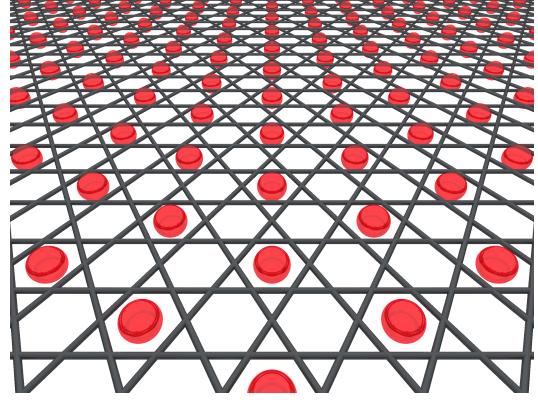

Figure 1. Sketch of the crystal of localized magnons (of minimal size) on the kagomé lattice antiferromagnet. These localized magnons (red discs) are superpositions of spin flips of spins residing at the vertices of the confining basic hexagons of the kagomé lattice.

Heisenberg antiferromagnet (KHAF), that is a celebrated paradigm of highly frustrated quantum magnetism [2–5]. The corresponding Hamiltonian is given by

$$\underset{\sim}{H} = J \sum_{\{i<j\}} \vec{\underset{\sim}{s}}_i \cdot \vec{\underset{\sim}{s}}_j + g\mu_B B \sum_i \underset{\sim}{s}_i^z \ , J > 0 \ , \quad (1)$$

where the first term models the Heisenberg exchange between spins at nearest neighbor sites i and j and the second term provides the Zeeman splitting in an external magnetic field.

In addition to the widely debated character of the spin-liquid ground state (GS), the intriguing magnetization process of the KHAF has attracted much attention [1, 10, 13, 14, 26, 28, 29, 31–40]. The magnetization exhibits plateaus at certain fractions of the saturation magnetization, namely at $\mathcal{M}/\mathcal{M}_{\text{sat}} = 3/9 = 1/3$, 5/9, 7/9 and likely also at $\mathcal{M}/\mathcal{M}_{\text{sat}} = 1/9$ [34, 35].

In contrast to the semiclassical $\mathcal{M}/\mathcal{M}_{sat} = 1/3$ plateau in the triangular-lattice Heisenberg antiferromagnet, see, e.g., [41–43], the kagomé plateau states are quantum valence-bond states [13, 14, 28, 33–35]. Moreover, around the $\mathcal{M}/\mathcal{M}_{sat} = 7/9$–plateau the flat lowest one-magnon band [10] dominates the low-temperature physics and leads to the exotic properties mentioned above. Interestingly, the $\mathcal{M}/\mathcal{M}_{sat} = 7/9$ plateau state just below the jump to saturation is a magnon crystal that is the magnetic counterpart of the Wigner crystal of interacting electrons in two dimensions. Since the magnon crystal spontaneously breaks translational symmetry, a finite-temperature phase transition is possible. The challenge is to find appropriate theoretical tools to describe such a transition for the quantum many-body system at hand.

Remarkably, the very existence of a flat band allows a semi-rigorous analysis of the low-temperature physics, e.g., for most of the one-dimensional flat-band quantum spin systems including the sawtooth chain [14, 29, 30] and also for a few two-dimensional systems, such as the frustrated bilayer [6, 44, 45] as well as the Tasaki lattice [46]. Such a semi-rigorous analysis builds on the existence of compact localized many-magnon states, which form either a massively degenerate GS manifold at the saturation field B_{sat} or a huge set of low-lying excitations for $B \lesssim B_{sat}$ and $B \gtrsim B_{sat}$. For the KHAF, the compact localized many-magnon states live on non-touching hexagons [10], which can be mapped to hard hexagons on a triangular lattice [13, 14, 26, 29]. This situation is depicted in Fig. 1.

On the experimental side the growing number of kagomé compounds is promising with respect to possible solid-state realizations of the kagomé flat-band physics [47–55]. Very recently the magnetization process in high field was reported for Cd-kapellasite [1]. The authors interpret the observed plateau states "as crystallizations of emergent magnons localized on the hexagon of the kagomé lattice". We will address the relation to our investigations in the discussion below.

Reliable predictions of the field–temperature regions where the magnon-crystal phase exists are useful to stimulate specific experiments. However, the semi-rigorous analysis of the flat-band properties of the KHAF based on compact localized many-magnon states, i.e., the hard-hexagon approximation (HHA) is limited because of the existence of a macroscopic number of additional *non-compact* localized many-magnon states [27]. A complete description can be given in terms of a loop gas (LG) that we elaborate in the Supplemental Material [56]. Moreover, at non-zero temperature also non-localized eigenstates influence the thermodynamics of the KHAF.

Numerical method.—To investigate the KHAF near the saturation field we present large-scale finite-temperature Lanczos (FTL) studies for finite lattices of $N = 27, \ldots 72$ sites, where we have selected only lattices exhibiting the magnon-crystal plateau at $\mathcal{M}/\mathcal{M}_{sat} =$
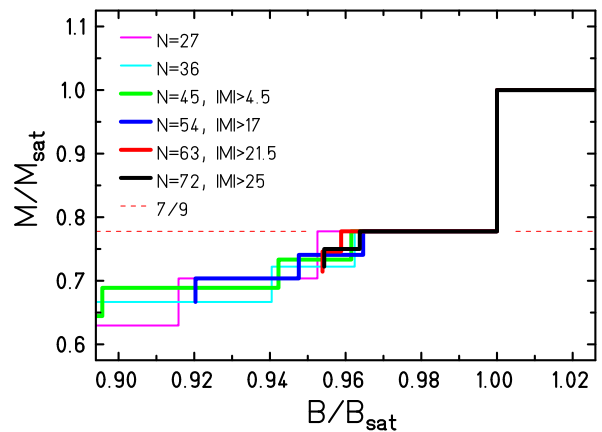

Figure 2. Magnetization $\mathcal{M}/\mathcal{M}_{sat}$: Region of the 7/9 plateau for various finite-size realizations of the KHAF.

7/9, which excludes $N = 42$ discussed in [37]. FTL is an unbiased numerical approach by which thermodynamic quantities are very accurately approximated by means of trace estimators [57–62]. Moreover, the consideration of six different lattices up to $N = 72$ allows to estimate finite-size effects. For used lattices and technical details see [56]. The kagomé lattices of N sites correspond to triangular lattices of $N_{trian} = N/3$ sites. On symmetry grounds, triangular lattices of $N_{trian} = 9, 12, 21$, *i.e.*, $N = 27, 36, 63$ sites seem to be most appropriate for our investigation [56, 63].

Results.—The magnetization curve around the 7/9–plateau and the jump to saturation are shown in Fig. 2. The size-independence of the height of the jump is obvious. The width of the plateau, i.e., the field region where the magnon-crystal phase can exist, is about 4% of the saturation field and its finite-size dependence is weak, cf. Ref. [35]. The finite-temperature transition to the magnon-crystal phase can be driven either by temperature when fixing B in the plateau region or by the magnetic field when fixing T below the critical temperature T_c. $C(B,T)$ is an appropriate quantity to detect the transition. For finite lattices the specific heat will not exhibit a true singularity, rather we may expect a well-pronounced peak in C that indicates the critical point. Furthermore, the peak has to become sharper with increasing N.

First, we study the temperature profile $C(T)$ for a magnetic field slightly below saturation, $B = 0.99\,B_{sat}$ (see Fig. 3). While the influence of N on the peak position T_{max} is rather weak, the increase of the height C_{max} with growing N is significant and the peaks are sharpest for $N = 63$ and $N = 72$.

Figure 4 presents a closer look at the results of Fig. 3 in terms of some characteristic quantities where we include the HHA [13, 14] and the LG description [56] for comparison. In panel (a) we first present a comparison of the total ground-state entropy per site. Since hard hexagons
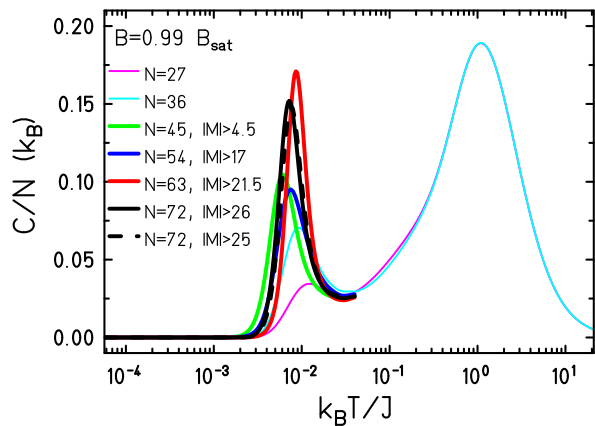
Figure 3. Specific heat for $B = 0.99B_{\text{sat}}$ for various finite-size realizations of the KHAF. For $N = 45, 54, 63, 72$, where too large Hilbert subspaces had to be neglected, only the low-temperature part of the specific heat is displayed; it is virtually correct for all system sizes.
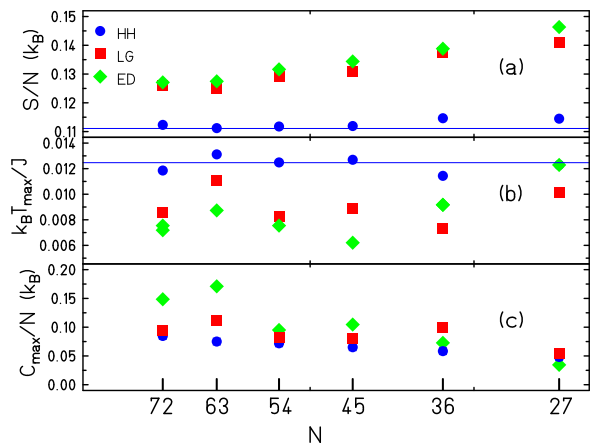

Figure 4. System-size dependence of several characteristic quantities at $B = 0.99\,B_{\text{sat}}$ for HH, LG, and ED: (a) entropy per site S/N associated to the total ground-state degeneracy, (b) position of the maximum of the specific heat T_{max}, and (c) value of the maximum of the specific heat per site C_{max}/N. The horizontal blue lines in panels (a) and (b) show the known thermodynamic limit for hard hexagons [13, 14, 64, 65].

are a subset of the loop configurations that in turn are a subset of the KHA ground states, the values of S increase correspondingly for a fixed N. For the HHA, the result for the thermodynamic limit is known [13, 14, 64] and shown by the horizontal blue line. We note that the result for $N = 63$ within the HHA approximation is very close to this $N = \infty$ limit. Since the finite-size effects of the LG and the KHA are very similar to that of the HHA, we assume that also for these models a system size of $N \geq 63$ is at least necessary to arrive at trustworthy results. It is thus a major achievement that by means of FTL such sizes are accessible.

We observe furthermore that nested loop configurations do indeed give rise to another macroscopic contribution to the ground states [27], and while this is approaching the ED result for the KHA, there is yet another contribution to the ground-state manifold that does not come from localized magnons and thus cannot be captured by the LG either.

Figure 4(b) displays the size dependence of the position of the maximum T_{max} of the specific heat in all three approximations. The thermodynamic limit of the HHA is again known [13, 14, 65] and again shown by the horizontal blue line. The positions for $N \gtrsim 45$ scatter around this value, and since the finite-size effects of all three approaches are again similar, we assume the same to be true for the LG and the KHA. Thus, we conclude that the critical temperature is lowered by the higher ground-state degeneracy of the LG and the KHA by up to 50% as compared to the HHA even for a field as close to the saturation field as $B = 0.99\,B_{\text{sat}}$.

Finally, Fig. 4(c) shows the size dependence of C_{max}/N. The range of accessible system sizes and lattice geometries is too small to reliably extract critical exponents, but one does observe a trend of C_{max}/N to grow
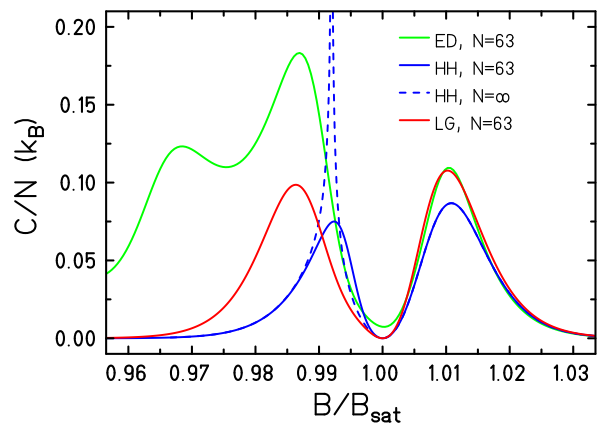

Figure 5. Specific heat vs. B at $T/J = 0.01$ for the KHAF, HH, and LG with $N = 63$ (solid curves) and the thermodynamic limit of hard hexagons [13, 14, 65] (dashed curve).

with increasing system size N. To be more precise, the transition is expected to belong to the universality class of the classical two-dimensional Potts model [13, 14] for all three cases. Thus, the asymptotic behavior of C_{max}/N for large N should be given by $C_{\text{max}}/N \propto N^{(\alpha/2\nu)}$[66] with critical indices $\alpha = 1/3$ and $\nu = 5/6$ [67, 68].

Next, we consider the field dependence of the specific heat for a representative low temperature $T/J = 0.01$, see Fig. 5, where we present data for $N = 63$ (solid curves). For the HHA, we include the result for the thermodynamic limit $N = \infty$ [13, 14, 65] (dashed curve). We note that both the HHA and the LG scale with $(B - B_{\text{sat}})/T$ [13, 14, 26]. There are two peaks left and right of the minimum in $C(B)$ at $B = B_{\text{sat}}$ which are related to the ground states of Fig. 4(a). The curves for
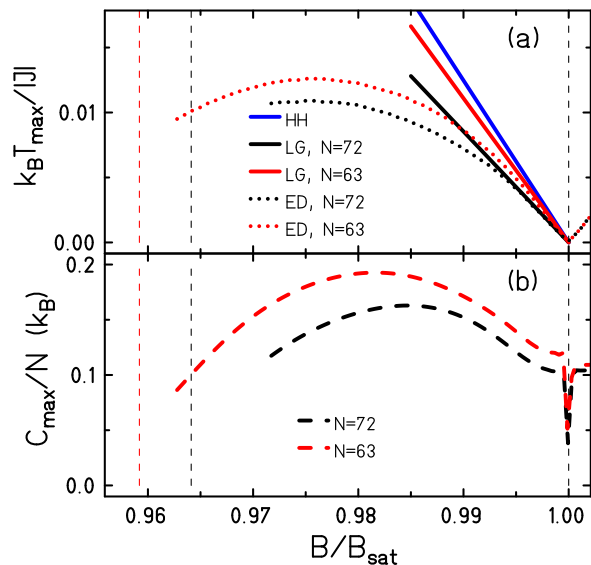
Figure 6. Phase diagram: (a) Position $T_{\max}$ and (b) height $C_{\max}$ of the low-T maximum (cf. Fig. 3) in dependence on B for $N = 63$ and $N = 72$ for fields where the maximum can be unambiguously detected. The vertical dashed lines mark the repective edges of the magnetization plateau.

$N = 63$ and ∞ of the HHA for the peak of $B > B_{\mathrm{sat}}$ are indistinguishable, showing that this is not a phase transition. The peaks of the LG and and ED for $B > B_{\mathrm{sat}}$ are at almost the same position but higher than for the HHA, and they do not signal a phase transition either. Remarkably, the LG is very close to the ED result for $B > B_{\mathrm{sat}}$, a fact that can be attributed to the LG reproducing the exact ground-state degeneracy of the highest sectors of total magnetic quantum number for the KHAF, see also [56].

Turning to the region $B < B_{\mathrm{sat}}$ of Fig. 5, here the HHA is known to exhibit a phase transition [13, 14, 65] whose location is given by the divergence of the $N = \infty$ curve (dashed). The peaks in the ED and LG curves just below $0.99\,B_{\mathrm{sat}}$ should correspond to the same crystallization transition, they are just rounded off by the finite size and pushed to lower B compared to the HHA by the larger number of states involved. In this region, the ED peak is higher than that of the LG. This difference is not only due to the KHAF having ground states that have no LG description [56], but also due to low-lying excitations. The latter give rise to a second peak at $0.97\,B_{\mathrm{sat}}$ that is present only in the ED data.

To derive a tentative phase diagram, we show in Fig. 6(a) the position $T_{\max}$ of the low-T peak of $C(T)$ vs B for $N = 63$ and $N = 72$. We also show the HHA result $T_c = 0.928(1 - B/B_{\mathrm{sat}})$ for $N = \infty$ [13, 14] and the LG curves for $N = 63$ and 72 (straight lines). The LG curves are very close to tangential to the corresponding ED results just below the saturation field, while the HHA yields a higher transition temperature, as already

noticed in the context of Fig. 4(b). As B decreases, the ED curves bend down, and when approaching the lower endpoint B_{end} of the plateau (depicted by the vertical lines in Fig. 6) $T_{\max}$ decreases and we may expect that it vanishes near B_{end}, where the magnon-crystal ground state disappears. For finite systems, as approaching B_{end} the relevant peak in $C(T)$ merges with low-T finite-size peaks appearing just below B_{end}, this way masking the true behavior expected for $N \to \infty$.

We mention that the general shape of the transition curve in Fig. 6(a) resembles the phase diagram of the magnon crystallization of the fully frustrated bilayer AFM [6, 44, 45]. Therefore, we may argue that the shape of this curve is generic for two-dimensional spin models possessing flat-band multi-magnon ground states.

The height of the maximum $C_{\max}$ of $C(T)$ (supposed to become a power-law singularity for $N \to \infty$) is shown in Fig. 6(b) vs B for $N = 63$ and $N = 72$. The shape of these curves is dome-like with a maximum near the midpoint of the plateau. The unusual behavior at $B = B_{\mathrm{sat}}$ is discussed in Ref. [26].

Discussion.—Our FTL data confirm the very existence of a low-temperature magnon-crystal phase just below the saturation field as conjectured by the HHA [13, 14]. However, the B–T region where this phase exists is not properly described by the HHA. Instead we elaborated a LG description that complements our FTL investigations. It is very accurate for $B > B_{\mathrm{sat}}$ and still yields a good description just below B_{sat}. Our investigations therefore provide guidance in which range of field and temperature a magnon-crystal phase is to be expected.

Coming back to the "magnon crystallization" reported in the experimental paper [1]: Here the authors interpret the observed plateau states "as crystallizations of emergent magnons localized on the hexagon of the kagomé lattice". This concept coincides with the present study for the 7/9–plateau, but may differ for plateaus at smaller magnetization, e.g., at 1/3 and 5/9. Although these lower plateaus can be understood as magnon crystals formed at $T = 0$, it still has to be investigated whether the physical behavior for $T > 0$ differs from the scenario discussed in this Letter, since the huge set of flat-band multi-magnon states determining the low-T thermodynamics near B_{sat} is missing for these plateaus.

As already discussed by the authors of [1] a real compound always differs from the idealized theoretical case for instance due to long-range dipolar or Dzyaloshinskii-Moriya interactions. In the case of Cd-kapellasite these seem to stabilize a phase at 10/12 of the saturation magnetization. However, the structure of this phase appears to be rather similar to that at 7/9, it therefore served as a strong motivation to investigate the possibility of a magnon crystallization phase transition on very general grounds (and with an idealized Hamiltonian). The effect of certain anisotropic Hamiltonians on magnon crystal phases confined to kagomé stripes is extensively discussed

in e.g. [40].

———————————

[*] jschnack@uni-bielefeld.de
[†] andreas.honecker@cyu.fr
[‡] Johannes.Richter@physik.uni-magdeburg.de

[1] R. Okuma, D. Nakamura, T. Okubo, A. Miyake, A. Matsuo, K. Kindo, M. Tokunaga, N. Kawashima, S. Takeyama, and Z. Hiroi, "A series of magnon crystals appearing under ultrahigh magnetic fields in a kagomé antiferromagnet," Nat. Commun. **10**, 1229 (2019).

[2] Leon Balents, "Spin liquids in frustrated magnets," Nature **464**, 199 (2010).

[3] Oleg A. Starykh, "Unusual ordered phases of highly frustrated magnets: a review," Rep. Prog. Phys. **78**, 052502 (2015).

[4] Philippe Mendels and Fabrice Bert, "Quantum kagome frustrated antiferromagnets: One route to quantum spin liquids," Comptes Rendus Physique **17**, 455 – 470 (2016).

[5] Lucile Savary and Leon Balents, "Quantum spin liquids," Rep. Prog. Phys. **80**, 016502 (2017).

[6] Johannes Richter, Olesia Krupnitska, Vasyl Baliha, Taras Krokhmalskii, and Oleg Derzhko, "Thermodynamic properties of $Ba_2CoSi_2O_6Cl_2$ in a strong magnetic field: Realization of flat-band physics in a highly frustrated quantum magnet," Phys. Rev. B **97**, 024405 (2018).

[7] Andreas Mielke, "Ferromagnetic ground states for the Hubbard model on line graphs," J. Phys. A: Math. Gen. **24**, L73–L77 (1991).

[8] Hal Tasaki, "Ferromagnetism in the Hubbard models with degenerate single-electron ground states," Phys. Rev. Lett. **69**, 1608–1611 (1992).

[9] Jürgen Schnack, Heinz-Jürgen Schmidt, Johannes Richter, and Jörg Schulenburg, "Independent magnon states on magnetic polytopes," Eur. Phys. J. B **24**, 475 (2001).

[10] Jörg Schulenburg, Andreas Honecker, Jürgen Schnack, Johannes Richter, and Heinz-Jürgen Schmidt, "Macroscopic magnetization jumps due to independent magnons in frustrated quantum spin lattices," Phys. Rev. Lett. **88**, 167207 (2002).

[11] Blundell, S. A. and Núñez-Regueiro, M. D., "Quantum topological excitations: from the sawtooth lattice to the Heisenberg chain," Eur. Phys. J. B **31**, 453–456 (2003).

[12] Johannes Richter, Jörg Schulenburg, Andreas Honecker, Jürgen Schnack, and Heinz-Jürgen Schmidt, "Exact eigenstates and macroscopic magnetization jumps in strongly frustrated spin lattices," J. Phys.: Condens. Matter **16**, S779 (2004).

[13] M. E. Zhitomirsky and Hirokazu Tsunetsugu, "Exact low-temperature behavior of a kagomé antiferromagnet at high fields," Phys. Rev. B **70**, 100403 (2004).

[14] M. E. Zhitomirsky and Hirokazu Tsunetsugu, "High field properties of geometrically frustrated magnets," Prog. Theor. Phys. Suppl. **160**, 361–382 (2005).

[15] Sebastian D. Huber and Ehud Altman, "Bose condensation in flat bands," Phys. Rev. B **82**, 184502 (2010).

[16] Siddharth A. Parameswaran, Rahul Roy, and Shivaji L. Sondhi, "Fractional quantum Hall physics in topological flat bands," Comptes Rendus Physique **14**, 816 – 839 (2013).

[17] E. J. Bergholtz and Z. Liu, "Toplogical flat band models and fractional Chern insulators," Int. J. Mod. Phys. B **27**, 1330017 (2013).

[18] Daniel Leykam, Sergej Flach, Omri Bahat-Treidel, and Anton S. Desyatnikov, "Flat band states: Disorder and nonlinearity," Phys. Rev. B **88**, 224203 (2013).

[19] Oleg Derzhko, Johannes Richter, and Mykola Maksymenko, "Strongly correlated flat-band systems: The route from Heisenberg spins to Hubbard electrons," Int. J. Mod. Phys. B **29**, 1530007 (2015).

[20] Daniel Leykam, Alexei Andreanov, and Sergej Flach, "Artificial flat band systems: from lattice models to experiments," Advances in Physics: X **3**, 1473052 (2018).

[21] Gyu-Boong Jo, Jennie Guzman, Claire K. Thomas, Pavan Hosur, Ashvin Vishwanath, and Dan M. Stamper-Kurn, "Ultracold atoms in a tunable optical kagome lattice," Phys. Rev. Lett. **108**, 045305 (2012).

[22] J. Struck, C. Ölschläger, M. Weinberg, P. Hauke, J. Simonet, A. Eckardt, M. Lewenstein, K. Sengstock, and P. Windpassinger, "Tunable gauge potential for neutral and spinless particles in driven optical lattices," Phys. Rev. Lett. **108**, 225304 (2012).

[23] Rodrigo A. Vicencio, Camilo Cantillano, Luis Morales-Inostroza, Bastián Real, Cristian Mejía-Cortés, Steffen Weimann, Alexander Szameit, and Mario I. Molina, "Observation of localized states in Lieb photonic lattices," Phys. Rev. Lett. **114**, 245503 (2015).

[24] Sebabrata Mukherjee, Alexander Spracklen, Debaditya Choudhury, Nathan Goldman, Patrik Öhberg, Erika Andersson, and Robert R. Thomson, "Observation of a localized flat-band state in a photonic Lieb lattice," Phys. Rev. Lett. **114**, 245504 (2015).

[25] F. Baboux, L. Ge, T. Jacqmin, M. Biondi, E. Galopin, A. Lemaître, L. Le Gratiet, I. Sagnes, S. Schmidt, H. E. Türeci, A. Amo, and J. Bloch, "Bosonic condensation and disorder-induced localization in a flat band," Phys. Rev. Lett. **116**, 066402 (2016).

[26] Oleg Derzhko and Johannes Richter, "Universal low-temperature behavior of frustrated quantum antiferromagnets in the vicinity of the saturation field," Eur. Phys. J. B **52**, 23–36 (2006).

[27] O. Derzhko, J. Richter, A. Honecker, and H.-J. Schmidt, "Universal properties of highly frustrated quantum magnets in strong magnetic fields," Low Temp. Phys. **33**, 745–756 (2007).

[28] Johannes Richter, Oleg Derzhko, and Jörg Schulenburg, "Magnetic-field induced spin-Peierls instability in strongly frustrated quantum spin lattices," Phys. Rev. Lett. **93**, 107206 (2004).

[29] Oleg Derzhko and Johannes Richter, "Finite low-temperature entropy of some strongly frustrated quantum spin lattices in the vicinity of the saturation field," Phys. Rev. B **70**, 104415 (2004).

[30] M. E. Zhitomirsky and Andreas Honecker, "Magnetocaloric effect in one-dimensional antiferromagnets," J. Stat. Mech.: Theor. Exp. , P07012 (2004).

[31] Kazuo Hida, "Magnetization process of the $S = 1$ and 1/2 uniform and distorted kagome Heisenberg antiferromagnets," J. Phys. Soc. Jpn. **70**, 3673 (2001).

[32] Andreas Honecker, Jörg Schulenburg, and Johannes Richter, "Magnetization plateaus in frustrated antiferromagnetic quantum spin models," J. Phys.: Condens. Matter **16**, S749 (2004).

[33] D. C. Cabra, M. D. Grynberg, P. C. W. Holdsworth, Andreas Honecker, P. Pujol, Johannes Richter, D. Schmalfuß, and Jörg Schulenburg, "Quantum kagomé antiferromagnet in a magnetic field: Low-lying nonmagnetic excitations versus valence-bond crystal order," Phys. Rev. B **71**, 144420 (2005).

[34] Satoshi Nishimoto, Naokazu Shibata, and Chisa Hotta, "Controlling frustrated liquids and solids with an applied field in a kagome Heisenberg antiferromagnet," Nat. Commun. **4**, 2287 (2013).

[35] Sylvain Capponi, Oleg Derzhko, Andreas Honecker, Andreas M. Läuchli, and Johannes Richter, "Numerical study of magnetization plateaus in the spin-$\frac{1}{2}$ kagome Heisenberg antiferromagnet," Phys. Rev. B **88**, 144416 (2013).

[36] Hiroki Nakano and Toru Sakai, "Numerical-diagonalization study of magnetization process of frustrated spin-1/2 Heisenberg antiferromagnets in two dimensions: Triangular- and kagome-lattice antiferromagnets," J. Phys. Soc. Jpn. **87**, 063706 (2018).

[37] Jürgen Schnack, Jörg Schulenburg, and Johannes Richter, "Magnetism of the $N = 42$ kagome lattice antiferromagnet," Phys. Rev. B **98**, 094423 (2018).

[38] Xi Chen, Shi-Ju Ran, Tao Liu, Cheng Peng, Yi-Zhen Huang, and Gang Su, "Thermodynamics of spin-1/2 kagome Heisenberg antiferromagnet: algebraic paramagnetic liquid and finite-temperature phase diagram," Science Bulletin **63**, 1545 – 1550 (2018).

[39] Katsuhiro Morita, Takanori Sugimoto, Shigetoshi Sota, and Takami Tohyama, "Magnetization plateaus in the spin-$\frac{1}{2}$ antiferromagnetic Heisenberg model on a kagome-strip chain," Phys. Rev. B **97**, 014412 (2018).

[40] S. Acevedo, C. A. Lamas, M. Arlego, and P. Pujol, "Magnon crystals and magnetic phases in a kagome-stripe antiferromagnet," Phys. Rev. B **100**, 195145 (2019).

[41] A. V. Chubukov and D. I. Golosov, "Quantum theory of an antiferromagnet on a triangular lattice in a magnetic field," J. Phys.: Condens. Matter **3**, 69 (1991).

[42] Andreas Honecker, "A comparative study of the magnetization process of two-dimensional antiferromagnets," J. Phys.: Condens. Matter. **11**, 4697 (1999).

[43] D. J. J. Farnell, R Zinke, Jörg Schulenburg, and Johannes Richter, "High-order coupled cluster method study of frustrated and unfrustrated quantum magnets in external magnetic fields," J. Phys.: Condens. Matter **21**, 406002 (2009).

[44] Fabien Alet, Kedar Damle, and Sumiran Pujari, "Sign-problem-free Monte Carlo simulation of certain frustrated quantum magnets," Phys. Rev. Lett. **117**, 197203 (2016).

[45] Oleg Derzhko, Taras Krokhmalskii, and Johannes Richter, "Emergent Ising degrees of freedom in frustrated two-leg ladder and bilayer $s = \frac{1}{2}$ Heisenberg antiferromagnets," Phys. Rev. B **82**, 214412 (2010).

[46] M. Maksymenko, A. Honecker, R. Moessner, J. Richter, and O. Derzhko, "Flat-band ferromagnetism as a Pauli-correlated percolation problem," Phys. Rev. Lett. **109**, 096404 (2012).

[47] J. L. Atwood, "Kagome lattice - a molecular toolkit for magnetism," Nat. Mater. **1**, 91–92 (2002).

[48] P. Mendels, F. Bert, M. A. de Vries, A. Olariu, A. Harrison, F. Duc, J. C. Trombe, J. S. Lord, A. Amato, and C. Baines, "Quantum magnetism in the paratacamite family: Towards an ideal kagomé lattice," Phys. Rev. Lett. **98**, 077204 (2007).

[49] F. Bert, S. Nakamae, F. Ladieu, D. L'Hôte, P. Bonville, F. Duc, J.-C. Trombe, and P. Mendels, "Low temperature magnetization of the $S = \frac{1}{2}$ kagome antiferromagnet $ZnCu_3(OH)_6Cl_2$," Phys. Rev. B **76**, 132411 (2007).

[50] Yoshihiko Okamoto, Masashi Tokunaga, Hiroyuki Yoshida, Akira Matsuo, Koichi Kindo, and Zenji Hiroi, "Magnetization plateaus of the spin-$\frac{1}{2}$ kagome antiferromagnets volborthite and vesignieite," Phys. Rev. B **83**, 180407 (2011).

[51] T.-H. Han, J. S. Helton, S. Chu, D. G. Nocera, J. A. Rodriguez-Rivera, C. Broholm, and Y. S. Lee, "Fractionalized excitations in the spin-liquid state of a kagome-lattice antiferromagnet," Nature **492**, 406–410 (2012).

[52] Kazuya Katayama, Nobuyuki Kurita, and Hidekazu Tanaka, "Quantum phase transition between disordered and ordered states in the spin-$\frac{1}{2}$ kagome lattice antiferromagnet $(Rb_{1-x}Cs_x)_2Cu_3SnF_{12}$," Phys. Rev. B **91**, 214429 (2015).

[53] H. Ishikawa, M. Yoshida, K. Nawa, M. Jeong, S. Krämer, M. Horvatić, C. Berthier, M. Takigawa, M. Akaki, A. Miyake, M. Tokunaga, K. Kindo, J. Yamaura, Y. Okamoto, and Z. Hiroi, "One-third magnetization plateau with a preceding novel phase in volborthite," Phys. Rev. Lett. **114**, 227202 (2015).

[54] M. R. Norman, "Colloquium: Herbertsmithite and the search for the quantum spin liquid," Rev. Mod. Phys. **88**, 041002 (2016).

[55] M. Yoshida, K. Nawa, H. Ishikawa, M. Takigawa, M. Jeong, S. Krämer, M. Horvatić, C. Berthier, K. Matsui, T. Goto, S. Kimura, T. Sasaki, J. Yamaura, H. Yoshida, Y. Okamoto, and Z. Hiroi, "Spin dynamics in the high-field phases of volborthite," Phys. Rev. B **96**, 180413 (2017).

[56] Supplemental material.

[57] J. Jaklič and P. Prelovšek, "Lanczos method for the calculation of finite-temperature quantities in correlated systems," Phys. Rev. B **49**, 5065–5068 (1994).

[58] Jürgen Schnack and Oliver Wendland, "Properties of highly frustrated magnetic molecules studied by the finite-temperature Lanczos method," Eur. Phys. J. B **78**, 535–541 (2010).

[59] Oliver Hanebaum and Jürgen Schnack, "Advanced finite-temperature Lanczos method for anisotropic spin systems," Eur. Phys. J. B **87**, 194 (2014).

[60] Burkhard Schmidt and Peter Thalmeier, "Frustrated two dimensional quantum magnets," Phys. Rep. **703**, 1 – 59 (2017).

[61] Eva Pavarini, Erik Koch, Richard Scalettar, and Richard M. Martin, eds., "The physics of correlated insulators, metals, and superconductors," (2017) Chap. The Finite Temperature Lanczos Method and its Applications by P. Prelovšek, ISBN 978-3-95806-224-5, http://hdl.handle.net/2128/15283.

[62] Jürgen Schnack, Johannes Richter, and Robin Steinigeweg, "Accuracy of the finite-temperature Lanc-

zos method compared to simple typicality-based estimates," Phys. Rev. Research **2**, 013186 (2020).

[63] Bernard Bernu, Claire Lhuillier, and L. Pierre, "Signature of Néel order in exact spectra of quantum antiferromagnets on finite lattices," Phys. Rev. Lett. **69**, 2590 (1992).

[64] R. J. Baxter and S. K. Tsang, "Entropy of hard hexagons," J. Phys. A: Math. Gen. **13**, 1023–1030 (1980).

[65] R. J. Baxter, "Hard hexagons: exact solution," J. Phys. A: Math. Gen. **13**, L61–L70 (1980).

[66] Jae-Kwon Kim and D. P. Landau, "Corrections to finite-size-scaling in two dimensional Potts models," Physica A **250**, 362–372 (1998).

[67] F. Y. Wu, "The Potts model," Rev. Mod. Phys. **54**, 235–268 (1982).

[68] T. Nagai, Y. Okamoto, and W. Janke, "Crossover scaling in the two-dimensional three-state Potts model," Condens. Matter Phys. **16**, 23605 (2013).

Jürgen Schnack,[1] Jörg Schulenburg,[2] Andreas Honecker,[3] and Johannes Richter[4, 5]

[1]*Fakultät für Physik, Universität Bielefeld, Postfach 100131, D-33501 Bielefeld, Germany*
[2]*Universitätsrechenzentrum, Universität Magdeburg, D-39016 Magdeburg, Germany*
[3]*Laboratoire de Physique Théorique et Modélisation, CNRS UMR 8089,*
CY Cergy Paris Université, F-95302 Cergy-Pontoise Cedex, France
[4]*Institut für Physik, Universität Magdeburg, P.O. Box 4120, D-39016 Magdeburg, Germany*
[5]*Max-Planck-Institut für Physik Komplexer Systeme,*
Nöthnitzer Straße 38, D-01187 Dresden, Germany
(Dated: June 11, 2020)

I. LATTICES

Figure 1 shows the lattices employed in the present work. The green lines indicate periodic boundary conditions. Firstly, we note that the lattices with $N = 27, 36$, and 63 share the six-fold rotational symmetry of the infinite lattice around the center of a hexagon. Indeed, the kagomé lattice can be considered as a triangular lattice of $N_{\text{trian}} = N/3$ sites, decorated by a basis of triangles, and the corresponding effective triangular lattices with $N_{\text{trian}} = 9, 12$, and 21 are known to be favorable from a symmetry point of view [1].

Secondly, we note that the $N = 27, 45$, and 54 lattices have loops of length 6 wrapping around the boundaries.

II. MAGNETIC QUANTUM NUMBERS

The eigenstates of the model are characterized by the magnetic quantum number M belonging to the z-component $\underset{\sim}{s}^z$ of the total spin and the $\vec{k}$-vector of the translational symmetry. While for $N = 27$ and $N = 36$ we can take into account all sectors of $|M|$, for $N > 36$ we are restricted to sectors of larger $|M|$: $|M| > 9/2$ for $N = 45$, $|M| > 17$ for $N = 54$, $|M| > 43/2$ for $N = 63$, and $|M| > 26$ for $N = 72$, respectively. This restriction is not severe, since close to the saturation field the eigenstates with small $|M|$ become excited states with higher energy. Nevertheless, for $N > 36$ we are restricted to low enough temperatures to avoid substantial contributions of states with small $|M|$ to the partition function.

III. ED SIZE SCALING

Here would like to provide an additional figure, complementing Fig. 5 of the main text, that shows the field dependence of the specific heat at low temperatures $T/J = 0.005, 0.01, 0.02$, see Fig. 2, where we present ED data for $N = 36$ (dashed) and $N = 63$ (solid curves). There are two peaks left and right of the minimum in $C(B)$ at $B = B_{\text{sat}}$ which are related to the huge set of low-lying excitations. The peaks are sharp at very low

$T/J = 0.005$ and become broader with increasing T. The height of the maximum above B_{sat} is almost identical for $N = 36$ and $N = 63$; it does not correspond to a phase transition [2, 3], see also the main text.

IV. LOOP-GAS DESCRIPTION

One can map the localized magnons states in the high-field regime of the kagomé lattice to a *geometric* problem of loop configurations [3–7].

Let $|\uparrow \ldots \uparrow\rangle$ be the ferromagnetically polarized state of the spin-1/2 Heisenberg antiferromagnet on a kagomé lattice with N sites. Then one can construct exact eigenstates in the sector $S^z = N/2 - n_\ell$ using n_ℓ closed loops and

$$| \{\ell_i\}\rangle = \prod_{i=1}^{n_\ell} \left(\sum_{x_i \in \ell_i} (-1)^{x_i} \underset{\sim}{s}^-_{x_i} \right) |\uparrow \ldots \uparrow\rangle. \qquad (1)$$

Here $(-1)^{x_i}$ stands symbolically for an alternating sign along the loop ℓ_i. For illustration, Fig. 3 shows three configurations consisting of two loops on the $N = 36$ lattice. The top panel shows a configuration consisting of two loops of minimal length, *i.e.*, compact localized magnons, corresponding to a configuration with two hard hexagons.

A. Properties of loop configurations

In order for the states Eq. (1) to be exact eigenstates, the loop configurations must satisfy the following conditions:

1. The length $|\ell_i|$ of the loop ℓ_i must be even in order to accommodate the alternating sign of the wave function along it.

2. A "loop" of length 2 turning back on its tail is not allowed since it would leave a single flipped spin in two triangles and thus not lead to an exact eigenstate.
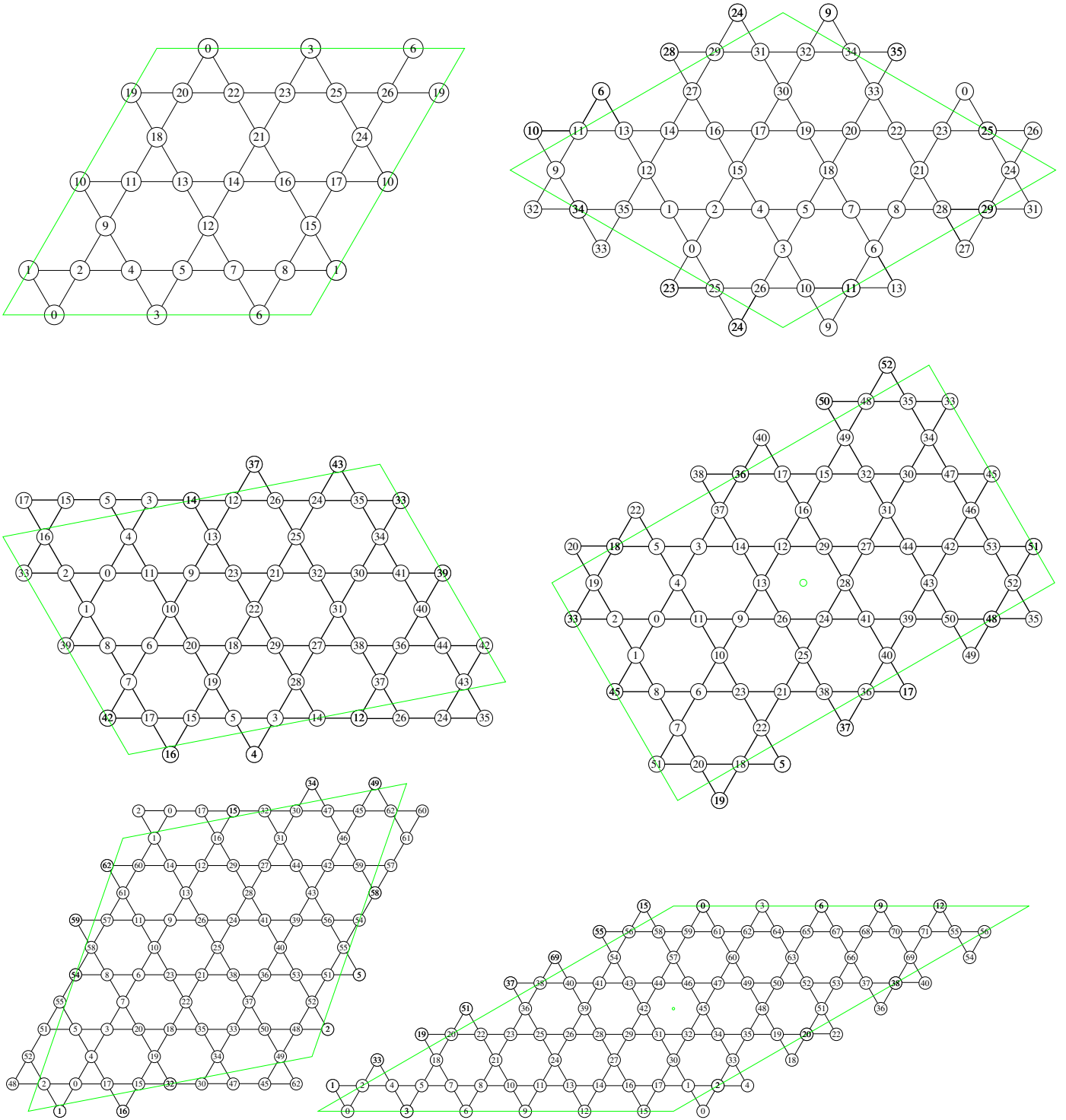
Figure 1. Finite kagomé lattices with $N = 27$, 36, 45, 54, 63, and $N = 72$ sites from top left to bottom right.

3. In each triangle, at most two sites are allowed to be occupied. This is required in order to ensure destructive interference when a spin flip wants to propagate outside a loop. This condition implies not only that a loop ℓ_i cannot approach itself too closely when turning back on itself, but also that

two loops ℓ_i and ℓ_j must be separated at least by one free site.

Actually, in order to ensure the exact eigenstate property of Eq. (1), exactly zero or two sites in each triangle must be occupied by a loop. Indeed, this is already ensured by the above rules. We further note that, at least for a
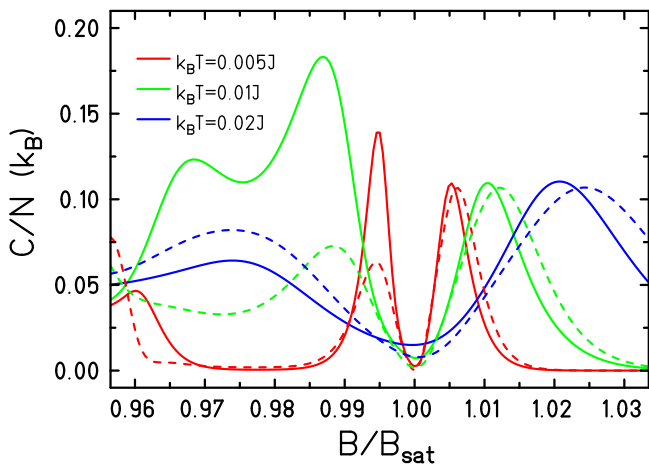
Figure 2. Specific heat vs. B at various low temperatures for the KHAF with $N = 63$ (solid curves) and $N = 36$ (dashed curves, same color for same temperature).

sufficiently big lattice, the shortest loops on the kagomé lattice have length $|\ell_i| = 6$. These include the loops winding around a hexagon, *i.e.*, the compact localized magnon states or "hard-hexagon" states. In addition, as mentioned in Sec. I, one may also have loops of length 6 winding around a periodic boundary.

The above rules can be implemented on a computer, thus allowing computer enumeration of the loop configurations for a finite lattice with N sites.

B. Linear relations

The wave functions Eq. (1) are not all linearly independent. For example, if the configurations $\{\ell_i\}$ and $\{\ell_i'\}$ differ by a loop $\ell_i' - \ell_i$ only in their ith factor and $(\ell_1, \ldots, \ell_{i-1}, \ell_i' - \ell_i, \ell_{i+1}, \ldots, \ell_{n_\ell})$ is also valid loop configuration, then $| \{\ell_i\}\rangle$, $| \{\ell_i'\}\rangle$, and $| \ell_1, \ldots, \ell_{i-1}, \ell_i' - \ell_i, \ell_{i+1}, \ldots, \ell_{n_\ell}\rangle$ are linearly dependent such that we may eliminate, e.g., $| \{\ell_i'\}\rangle$ from the spanning set.

For convenience, we recall what is known about the degeneracies of the ground-state manifold on an N-site kagomé lattice [3]:

- The degeneracy is known to be $N/3 + 1$ in the $n_\ell = 1$ sector. This is evident, e.g., from a band picture. An equivalent counting is $N/3$ hard hexagons, subject to one linear relation plus two winding states.

- In the sector corresponding to $n_\ell = 2$, the degeneracy is $(N-3)(N-6)/18$. Ref. [3] gave the following interpretation of this number: firstly, there are $N/6(N/3 - 7)$ configurations with two hard hexagons. Secondly, there are $2N/3$ independent configurations composed of one hard hexagon and a winding state. Thirdly, there is one further linearly independent state composed of two winding
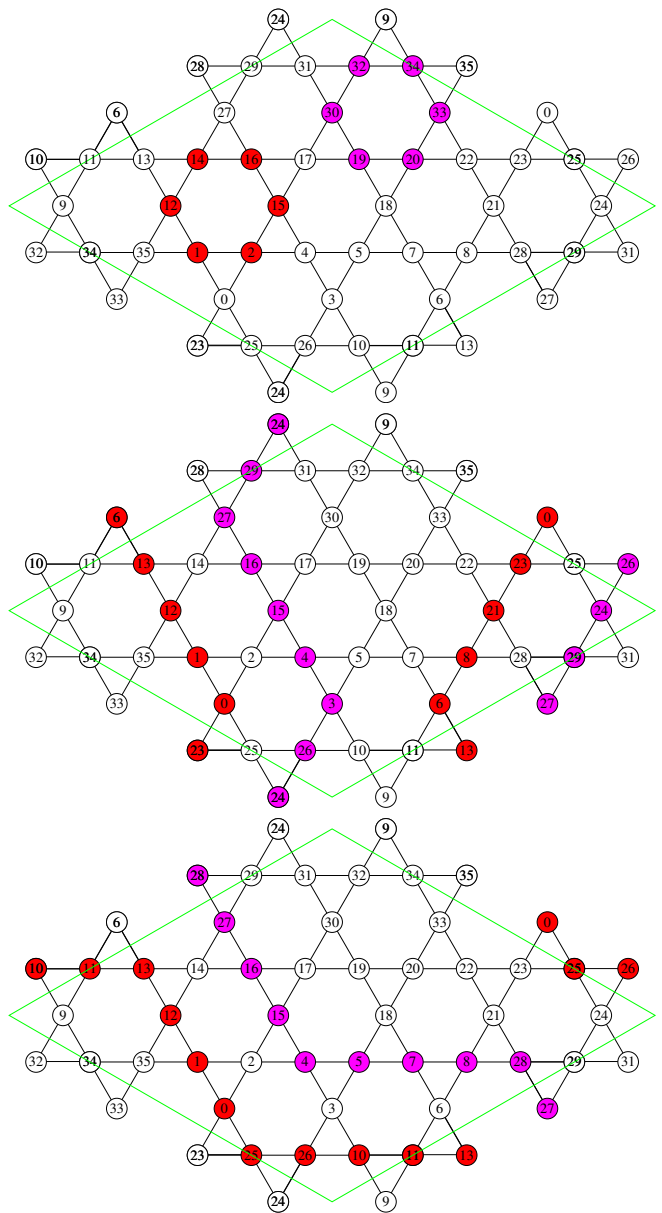

Figure 3. Top: Configuration with two minimal localized magnons (minimal loops) on the $N = 36$ kagomé lattice. Center and bottom: Two configurations with two loops winding around the boundary. The sites belonging to the two loops are shown by the filled red and magenta circles, respectively.

states.

The latter statement indicates that a purely geometric picture will be insufficient. To illustrate this point, we show in the center and bottom panel of Fig. 3 two double-winding configurations on an $N = 36$ kagomé lattice. Since the winding number is conserved by local moves, it is not possible to deform these two configurations into each other by local moves, or to reduce them to hard hexagons, neither to one hard hexagon and one winding configuration. Therefore, it will in general be necessary

to investigate the linear relations between the vectors Eq. (1).

The hard-hexagon configurations can still be considered to be linearly independent. On the torus created by the periodic boundary conditions, this is not strictly true, but the resulting linear relation can be compensated by adding a winding state.

In general, we determine the linear relations as follows. First, we note that the scalar product of two vectors of the type Eq. (1) can be computed within the loop representation. It is therefore not necessary to work in the possibly high-dimensional vector space of spin configurations with $S^z = N/2 - n_\ell$, but one can in fact perform a Gram-Schmidt orthogonalization in the abstract space of the states Eq. (1) and in this manner determine the dimension of the vector space spanned by them.

C. Results of computer enumeration

Tables I–VI summarize results obtained by computer enumeration and subsequent Gram-Schmidt orthogonalization for the lattices shown in Fig. 1. These tables include results for the Heisenberg model and hard hexagons, where for the convenience of the reader we also reproduce some data from Refs. [3, 8] in Tables II–V. The column quoting the total number of loop configurations is not very relevant for our present purposes, but it demonstrates the large number of allowed loop configurations, in particular in the single-loop sector ($n_\ell = 1$).

Firstly, for $N = 27$, $N = 45$, and 54 there are $N/9$ more 6-loop configurations than hard hexagons in the sector $n_\ell = 1$. Indeed, as already stated in Sec. I, one can see in Fig. 1 that there are loops of length 6 winding around the boundary. This implies also the existence of a fourth "magnon crystal" in the sector with $n_\ell = N/9$ consisting of these loops winding around the boundary, thus explaining why the degeneracy of the Heisenberg model in the sector with $S^z = 35/2$ and 21 respectively is found to be 4 on the $N = 45$ and 54 lattices, and not just 3 as expected from hard hexagons, see Tables III and IV.

Secondly, for most sectors with $n_\ell \geq 3$ the number of linearly independent loop configurations is smaller than the degeneracy of the corresponding sector of the Heisenberg model. This includes the sector $S^z = 14$ on the $N = 36$ lattice where the degeneracy is 8 while there are only 3 configurations consisting of 4 loops (see Table II). Consequently, some ground states of the Heisenberg model are evidently not captured by the loop picture; the biggest difference that we have observed is 648 non-loop ground states of the Heisenberg model in the sector $S^z = 31$, $n_\ell = 5$ on the $N = 72$ lattice, see Table VI. However, there are significantly more linearly independent loop configurations than simple hard-hexagon configurations such that the present picture amounts to an improved description of the ground-state manifold of the Heisenberg model.

There is a third intriguing observation pointing towards a significant difference between the $N = 63$ and $N = 72$ lattices. For $N = 63$ and in the sector $n_\ell = N/3 - 1 = 6$, there are exactly as many loop as hard-hexagon configurations, leaving no room for linear relations, see Table V. On the other hand, Table VI shows that in the corresponding case $n_\ell = N/3 - 1 = 7$ for $N = 72$, there are more than 3 times as many linearly independent loop as hard-hexagon configurations.

Figure 4(a) of the main manuscript characterizes the total ground-state degeneracy in terms of the associated entropy per site. We should mention that the $N = 72$ 'ED' data point in this figure is only a lower bound since we were so far not able to compute the ground-state degeneracy of the Heisenberg model in the sectors with $S^z \leq 30$, as specified by the missing entries in Table VI, such that in these cases we have used the number of linearly independent loop configurations as a lower bound.

D. Specific heat

From the multiplicities in Tables I–VI it is straightforward to compute thermodynamic properties such as the specific heat. We note that both for hard hexagons and the loop gas, the results depend only on $(B_{\text{sat}} - B)/T$ which plays the role of a chemical potential [2, 5, 7]. Nevertheless, for comparison with exact diagonalization (ED), we take a value of the magnetic field close to the saturation field, $B = 0.99 B_{\text{sat}}$. The results for the specific heat per site C/N are shown in Fig. 4 (here we set $k_B = 1$). This figure also includes the exact diagonalization results for the Heisenberg model from the main text. Although the behavior is somewhat irregular as a function of system size N, the loop-gas description is evidently in better agreement with the full Heisenberg model than the simpler hard-hexagon model. This concerns in particular the position of the low-temperature maximum where the loop gas and the Heisenberg model yield almost identical positions for $N = 54$ and 72. In order to emphasize this point even more, we show in the $N = 27, \ldots, 63$ panels in green the specific heat that is obtained when we take into account just the ground-state degeneracy of the Heisenberg model according to Tables I–V. Firstly, we see that the low-temperature peak of the specific heat is indeed dominated by the ground-state manifold, and that the loop gas yields in turn a rather accurate account of these. Nevertheless, one observes also that the full ED result for the low-temperature peak of the specific heat is clearly higher even than just the ground-state contribution. This can be understood from the gap Δ to the first excited state that is also included Tables I–VI. Indeed, this gap is so small, at least in some sectors, that even at a temperature as low as $T \approx J/100$ the contribution from thermally excited states to the specific heat is quantitatively relevant.

Generally, the maximum value of the specific heat remains smaller in the loop gas than in the full Heisenberg

Heisenberg model			loop gas			hard hexagons
S^z	degeneracy	gap Δ/J	n_ℓ	# confs.	# lin. indep.	# confs.
25/2	10	0.63397	1	783	10	9
23/2	28	0.20165	2	234	28	9
21/2	13	0.04379	3	6	6	3

Table I. Data for the $N = 27$ lattice. For the Heisenberg model, we quote the gap to the lowest excited state above the degenerate ground-state manifold in the corresponding sector of S^z.

Heisenberg model			loop gas			hard hexagons
S^z	degeneracy	gap Δ/J	n_ℓ	# confs.	# lin. indep.	# confs.
17	13	0.5	1	5442	13	12
16	55	0.18159	2	2616	55	30
15	71	0.05548	3	130	70	16
14	8	0.03363	4	3	3	3

Table II. Data for the $N = 36$ lattice. For the $S = 1/2$ Heisenberg model and the number of hard-hexagon configurations compare Ref. [3].

Heisenberg model			loop gas			hard hexagons
S^z	degeneracy	gap Δ/J	n_ℓ	# confs.	# lin. indep.	# confs.
43/2	16	0.25139	1	37221	16	15
41/2	91	0.12257	2	23530	91	60
39/2	201	0.03478	3	4520	190	60
37/2	110	0.01055	4	260	60	15
35/2	4	0.01176	5	4	4	3

Table III. Data for the $N = 45$ lattice. For the $S = 1/2$ Heisenberg model and the number of hard-hexagon configurations compare Ref. [3].

Heisenberg model			loop gas			hard hexagons
S^z	degeneracy	gap Δ/J	n_ℓ	# confs.	# lin. indep.	# confs.
26	19	0.17712	1	255696	19	18
25	136	0.09119	2	195975	136	99
24	430	0.02458	3	63036	413	180
23	513	0.00901	4	9192	396	99
22	119	0.00295	5	384	90	18
21	4	0.01237	6	4	4	3

Table IV. Data for the $N = 54$ lattice. For the $S = 1/2$ Heisenberg model and the number of hard-hexagon configurations compare Ref. [3].

Heisenberg model			loop gas			hard hexagons
S^z	degeneracy	gap Δ/J	n_ℓ	# confs.	# lin. indep.	# confs.
61/2	22	0.29675	1	1927644	22	21
59/2	190	0.12841	2	1743441	190	147
57/2	785	0.05004	3	481509	784	406
55/2	1436	0.02395	4	40656	1288	399
53/2	617	0.00629	5	1029	294	105
51/2	21	0.01132	6	21	21	21
49/2	3	0.04807	7	3	3	3

Table V. Data for the $N = 63$ lattice. For the $S = 1/2$ Heisenberg model in the sectors with $S^z \geq 57/2$ and the number of hard-hexagon configurations compare Ref. [3], for the degeneracy of the Heisenberg model in the $S^z = 49/2$ sector, compare Ref. [8].

model on the kagomé lattice (see also Fig. 4(c) of the main text). This is consistent with the number of linearly independent loop-gas states being lower than the number of independent ground states, see Tables I–VI and Fig. 4(a) of the main text. The exceptions to this general rule are the cases $N = 27$ and 36. The latter can be traced back to a difference of the number of ground states that for the case $N = 36$ are in the sector $S^z = 14$, $n_\ell = 4$: for the full Heisenberg model, this degeneracy is 8 while there are only 3 linearly independent loop-gas

Heisenberg model			loop gas			hard hexagons
S^z	degeneracy	gap Δ/J	n_ℓ	# confs.	# lin. indep.	# confs.
35	25	0.13397	1	12611908	25	24
34	253	0.07558	2	13519854	253	204
33	1293	0.02521	3	5961328	1293	752
32	3303	0.01013	4	1321624	3207	1218
31	3512	0.00462	5	133700	2864	816
30		0.00333	6	5894	954	212
29			7	120	84	24
28			8	3	3	3

Table VI. Data for the $N = 72$ lattice.

and hard-hexagon configurations, see Table II. A similar difference appears for $N = 27$, namely 13 versus 6, respectively 3 in the sector $S^z = 21/2$, $n_\ell = 3$, see Table I. Consequently, the leading term of the low-temperature expansion of the partition function Z is very different, thus giving rise to the significant differences in the low-temperature specific heat C/N that one observes in the panels for $N = 27$ and 36 of Fig. 4.

Figure 5 regroups this data for the specific heat according to method in order to expose the finite-size behavior more clearly (another presentation of the ED results is given in Fig. 3 of the main text). One sees in Fig. 5 that the hard-hexagon description yields a maximum that increases monotonically with increasing N (see also Fig. 4(c) of the main text). Here, the thermodynamic limit is known [5, 7, 9] such that we can include this result in the hard-hexagon panel. By contrast, both the loop-gas description and ED yield significantly less regular behavior. However, the changes as a function of N are very similar for the latter two methods, in particular when one goes from $N = 63$ to 72, the notable exceptions being again the cases $N = 27, 36$.

Overall, we conclude that the loop-gas description yields not only a substantial improvement over hard hexagons, but also that the $N = 63$ and 72 lattices are more representative of the generic behavior than the smaller lattices, thus underlining again also the importance of being able to access such big system sizes by FTL.

[1] Bernard Bernu, Claire Lhuillier, and L. Pierre, "Signature of Néel order in exact spectra of quantum antiferromagnets on finite lattices," Phys. Rev. Lett. 69, 2590 (1992).

[2] Oleg Derzhko and Johannes Richter, "Universal low-temperature behavior of frustrated quantum antiferromagnets in the vicinity of the saturation field," Eur. Phys. J. B 52, 23–36 (2006).

[3] O. Derzhko, J. Richter, A. Honecker, and H.-J. Schmidt, "Universal properties of highly frustrated quantum magnets in strong magnetic fields," Low Temp. Phys. 33, 745–756 (2007).

[4] Jörg Schulenburg, Andreas Honecker, Jürgen Schnack, Johannes Richter, and Heinz-Jürgen Schmidt, "Macroscopic magnetization jumps due to independent magnons in frustrated quantum spin lattices," Phys. Rev. Lett. 88, 167207 (2002).

[5] M. E. Zhitomirsky and Hirokazu Tsunetsugu, "Exact low-temperature behavior of a kagomé antiferromagnet at high fields," Phys. Rev. B 70, 100403 (2004).

[6] Johannes Richter, Jörg Schulenburg, Andreas Honecker, Jürgen Schnack, and Heinz-Jürgen Schmidt, "Exact eigenstates and macroscopic magnetization jumps in strongly frustrated spin lattices," J. Phys.: Condens. Matter 16, S779 (2004).

[7] M. E. Zhitomirsky and Hirokazu Tsunetsugu, "High field properties of geometrically frustrated magnets," Prog. Theor. Phys. Suppl. 160, 361–382 (2005).

[8] Sylvain Capponi, Oleg Derzhko, Andreas Honecker, Andreas M. Läuchli, and Johannes Richter, "Numerical study of magnetization plateaus in the spin-$\frac{1}{2}$ kagome Heisenberg antiferromagnet," Phys. Rev. B 88, 144416 (2013).

[9] R. J. Baxter, "Hard hexagons: exact solution," J. Phys. A: Math. Gen. 13, L61–L70 (1980).
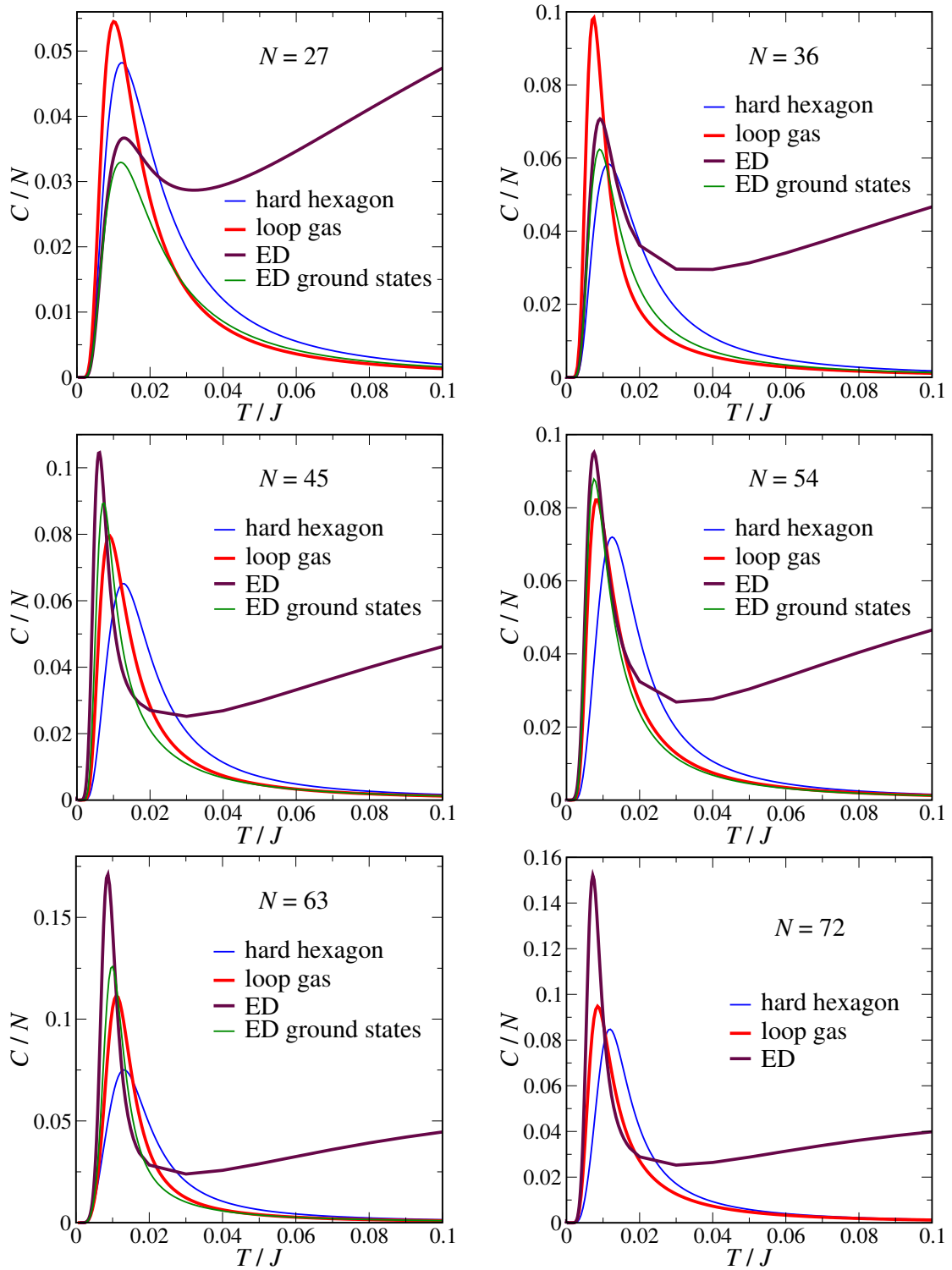
Figure 4. Specific heat per site C/N for the $N = 27, 36, 45, 54, 63$, and 72 lattices at $B = 0.99\,B_{\text{sat}}$. The green lines in the $N = 27, \dots, 63$ panels correspond to just taking the ground states of the Heisenberg model into account whose numbers are given in Tables I–V.
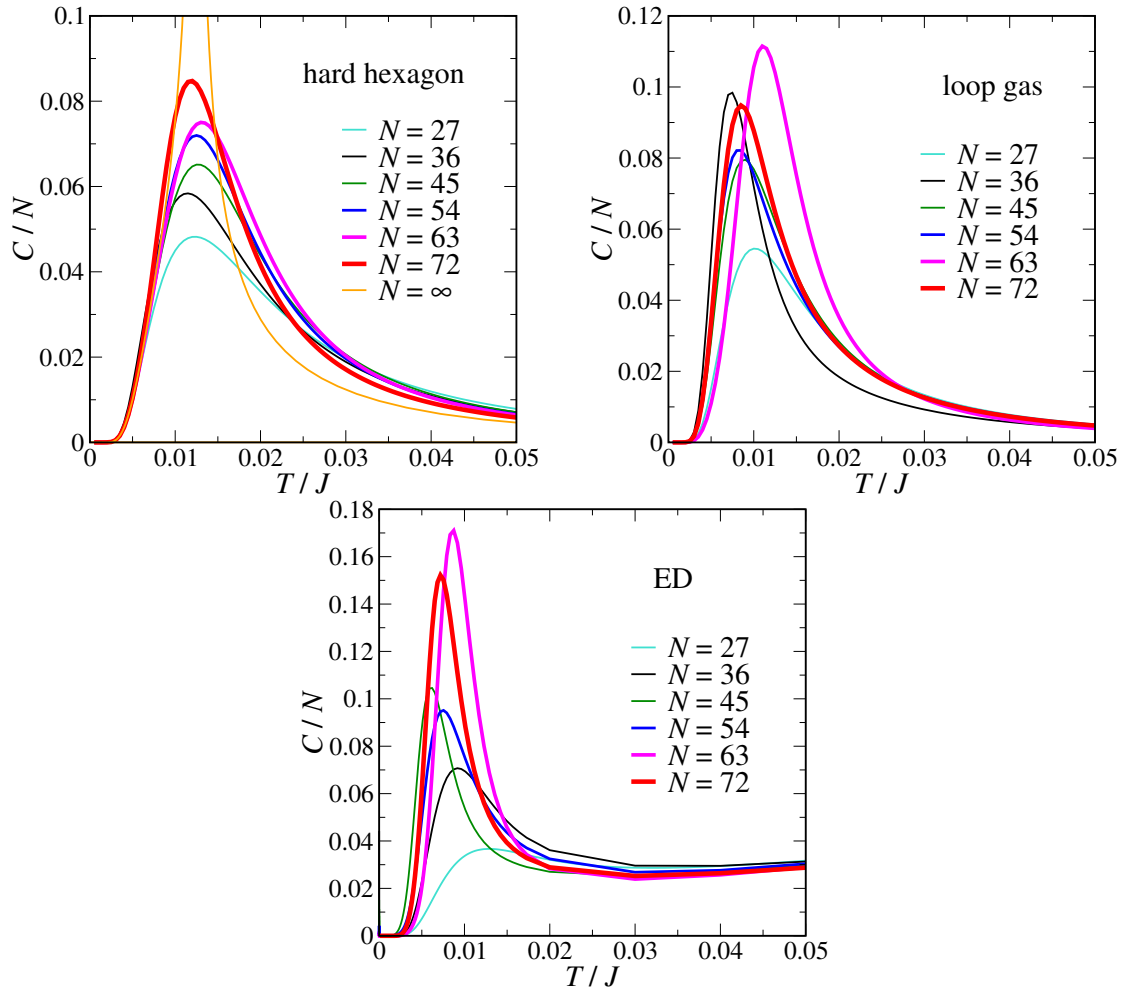
Figure 5. Same data as in Fig. 4, but grouped according to method rather than size N. The hard-hexagon panel includes also the result for the thermodynamic limit [5, 7, 9].